BIOCHEMISTRY

Ribosomal protein bL27 protects translating ribosomes from tmRNA-SmpB

Divyasorubini Seerpatham[1], George Wanes[2,3], Chathuri Pathirage[4], Mynthia Cabrera[5], Edu Usoro[6], Kristin S. Koutmou[4], Christine M. Dunham[6], Paul C. Whitford[2,3,7], Kenneth C. Keiler[1,8]*

Bacterial ribosomal protein bL27 is universally conserved, and its amino terminus is adjacent to the peptidyl transfer center, yet its roles in translation remain unclear. Combining genetics, biochemistry, and molecular dynamics, we show that bL27 has an unexpected role in preventing transfer-messenger RNA (tmRNA)-small protein B (SmpB), molecules involved in the trans-translation bacterial ribosome rescue mechanism, from interfering with protein synthesis. Deletion of the bL27 gene causes a 10,000-fold decrease in viability, and this defect is partially rescued by deletion of the gene encoding tmRNA. Addition of tmRNA-SmpB to in vitro translation reactions decreases the rate of protein synthesis by ribosomes lacking bL27 but has no effect on wild-type ribosomes. Molecular dynamics simulations also indicate that bL27 can slow the movement of tmRNA on the ribosome. These data link trans-translation and bL27 and support a model in which the amino terminus of bL27 acts as a gatekeeper to prevent tmRNA from sterically interfering with tRNA (transfer RNA) on the ribosome.

INTRODUCTION

The genes encoding ribosomal protein bL27 (*rpmA*), transfer-messenger RNA (tmRNA; *ssrA*), and small protein B (SmpB; *smpB*) are among the set conserved in almost all bacterial species but absent from metazoans. tmRNA and SmpB function together in the trans-translation pathway to rescue ribosomes that are stalled at the 3′ end of an mRNA (nonstop ribosomes) (*1*–*3*). During trans-translation, the C-terminal tail of SmpB binds in the empty mRNA channel of a nonstop ribosome, and the tmRNA-SmpB complex enters the decoding center of the ribosomal aminoacyl (A) site (*4*–*6*). A specialized reading frame within tmRNA is inserted into the mRNA channel, and translation resumes to add the tmRNA-encoded SsrA peptide to the end of the nascent polypeptide, ultimately releasing the ribosome at a normal stop codon (*7*–*12*). The rescue of nonstop ribosomes is essential in bacteria because damaged and truncated mRNAs are prevalent (*13*).

Trans-translation is essential for viability and virulence in numerous bacterial pathogens, making it a promising target for antibiotic development (*13*). A family of acylaminooxadiazole compounds, including KKL-2098, selectively inhibits trans-translation without disrupting normal translation (*14*, *15*). A single-particle cryo–electron microscopy structure of nonstop ribosomes bound with KKL-2098 showed that the inhibitor binds to a site near the premature termination codon (PTC) that is not targeted by other antibiotics (*14*). In this structure, the highly conserved N-terminal sequence of bL27 adopted a previously unobserved position (*14*). bL27 normally extends toward the PTC, and it is the closest protein to the catalytic site (*6*, *16*, *17*). The N-terminal sequence is not resolved in many structures that have an empty A site, suggesting that it is mobile when there is no A-site tRNA (*6*, *16*, *17*). In the structure with bound KKL-2098, the N-terminal sequence of bL27 is rotated ~180° away from the PTC by bending at residue Gly[8] (*14*). Displacement of bL27 was proposed to be important for inhibition by KKL-2098, and *Escherichia coli* carrying N-terminal truncations of bL27 was hypersensitive to the acylaminooxadiazole inhibitors, indicating that bL27 and trans-translation may be linked (*14*, *18*).

Despite the conservation of bL27 and its position adjacent to the PTC, its function is not known. On the basis of the proximity of bL27 to the PTC, bL27 was proposed to play a role in peptidyl transferase activity (*19*–*22*). However, more recent experiments show that removing bL27 from the ribosome does not change the catalytic rate (*23*). Mutation of the bL27 N-terminal sequence also has a minimal effect on tRNA selection, the rate of elongation, or the rate of peptide release during normal translation (*23*). Nevertheless, deletion of bL27 in *E. coli* results in slow growth, suggesting that bL27 has a critical function in protein production (*24*, *25*). Here, we demonstrate that deletion of tmRNA partially suppresses the growth phenotype caused by deletion of bL27, and addition of tmRNA-SmpB to in vitro translation reactions slows the rate of protein synthesis when bL27 is absent. Molecular dynamics simulations indicate that bL27 interferes with the entry of tmRNA-SmpB into the PTC but does not affect the dynamics of tRNA. On the basis of these data, we propose that a major role for bL27 is to prevent tmRNA-SmpB from interfering in normal protein synthesis.

RESULTS

Mutations in bL27 specifically increase trans-translation and susceptibility to trans-translation inhibitors

Because the N terminus of bL27 moves away from the PTC when KKL-2098 is bound, we hypothesized that this portion of bL27 might be required for trans-translation and inhibitors might function by displacing bL27 (*14*). To test these ideas, we made substitution and deletion mutations in the N terminus of bL27, or deleted bL27 entirely, and measured antibiotic susceptibility and trans-translation activity. The mutant with no bL27 was hypersensitive to trans-translation inhibitors KKL-35 and MBX-4132 (which are acylaminooxadiazoles similar to KKL-2098; fig. S2A), with median inhibitory concentration (IC_{50}) values ~50% of

[1]Department of Molecular Biosciences, University of Texas at Austin, Austin, TX, USA. [2]Center for Theoretical Biological Physics, Northeastern University, Boston, MA, USA. [3]Department of Physics, Northeastern University, Boston, MA, USA. [4]University of Michigan, Ann Arbor, MI, USA. [5]Department of Biochemistry and Molecular Biology, Pennsylvania State University, University Park, PA, USA. [6]Department of Chemistry, Emory University, Atlanta, GA, USA. [7]Department of Chemical Engineering, Northeastern University, Boston, MA, USA. [8]LaMontagne Center for Infectious Diseases, University of Texas at Austin, Austin, TX, USA.
*Corresponding author. Email: kkeiler@utexas.edu

the values measured for strains with wild-type bL27 (fig. S2B). Mutation of the broadly conserved HKK residues in bL27 (AHKKAGG to AaaaAGG; mutated residues shown in lowercase) increased susceptibility to an extent comparable to removing bL27 entirely (fig. S2B). Similarly, truncation of the N-terminal sequence by two, three, five, or six residues caused hypersensitivity (fig. S2B). In contrast, none of the bL27 mutants showed a statistically significant change in susceptibility to linezolid (fig. S2B), which binds near the PTC, or to tetracycline (fig. S2B), which binds the small subunit of the ribosome (*26*–*28*). The specific increase in susceptibility to acylaminooxadiazoles caused by bL27 mutations suggests that the N-terminal sequence of bL27 decreases the binding affinity or efficacy of these inhibitors.

To investigate the contribution of bL27 to trans-translation, we purified ribosomes from mutant strains and measured trans-translation in vitro with different concentrations of tmRNA-SmpB. Ribosomes from all strains produced SsrA-tagged dihydrofolate reductase (DHFR), indicating that bL27 is not essential for trans-translation (Fig. 1A). Dose-response experiments showed that the concentration of tmRNA-SmpB required to achieve half-maximal tagging activity (EC_{50}) on ribosomes with no bL27 or with the AaaaAGG mutant was <25% of the EC_{50} on ribosomes with wild-type bL27. These data indicate that tmRNA-SmpB interacts with mutant ribosomes more productively than those carrying wild-type bL27 (Fig. 1B).

To test whether peptidyl transfer to tmRNA is altered in ΔbL27 ribosomes, we assembled wild-type and ΔbL27 ribosomes on nonstop mRNA with ^{35}S-fMet-tRNA^{fMet} in the P site and added an alanine-charged tmRNA-SmpB-EF-Tu-GTP complex to the A site (Fig. 1C and fig. S3). The extent of peptidyl transfer to tmRNA was compared to translation on a canonical, stop codon–containing transcript. We find that similar levels of peptidyl transfer are achieved for wild-type ribosomes undergoing normal translation and trans-translation. In contrast, ΔbL27 ribosomes exhibit a nearly threefold increase in peptidyl transfer to tmRNA compared to the transfer to tRNA (Fig. 1C). Overall, these results suggest that wild-type bL27 interferes with both trans-translation and acylaminooxadiazole activity (*14*).

bL27 is a gatekeeper for tmRNA-SmpB movement on the ribosome

The lower EC_{50} for tmRNA-SmpB in the absence of bL27 suggests that the wild-type N-terminal sequence of bL27 may limit access of tmRNA-SmpB to the PTC. If that is true, there should be more trans-translation in cells lacking bL27. To test this prediction, we expressed a tmRNA variant that encodes a peptide tag ending in HHHHHHD (*29*). This tag does not target proteins for degradation, so tagged proteins can be observed using an anti-His tag antibody. Western blots loaded with equal amounts of total protein from wild-type and Δ*rpmA* strains showed that the fraction of protein containing the SsrA tag was substantially higher in the absence of bL27 (Fig. 1D). These data indicate that there is more trans-translation in cells lacking bL27, consistent with bL27 limiting the access of tmRNA-SmpB to the PTC.

Despite increased trans-translation on ΔbL27 ribosomes in vitro and in vivo, we find that trans-translation on these ribosomes still requires a truncated mRNA. We tested whether trans-translation could occur on ribosomes in the middle of an mRNA by repeating the in vitro assays using a DHFR template containing a stop codon at the 3′ end of the gene followed by a 33-nucleotide extension (DHFR-stop+33), while release factors (RFs) were omitted from the reaction to prevent termination. Previous experiments showed that when a wild-type ribosome stalls at the stop codon on DHFR-stop+33, the 33-nucleotide extension occupies the mRNA channel, preventing trans-translation (*30, 31*). Here, no trans-translation was observed with wild-type or ΔbL27 ribosomes on DHFR-stop+33 (Fig. 1E). These results suggest that substrate specificity is not radically altered in the ΔbL27 ribosomes and that the increased trans-translation observed in cells lacking bL27 is likely due to more productive trans-translation on nonstop ribosomes.

Because tmRNA-SmpB interacts more productively with bL27 mutant ribosomes, we asked whether normal translation is also increased on mutant ribosomes. We monitored protein production over 90 min from a DHFR template that contained a stop codon and found that ribosomes containing the AaaaAGG mutant bL27 produced approximately the same amount of DHFR as the wild-type ribosomes at all time points tested. This result indicates that mutation of the HKK residues of bL27 does not affect translation (Fig. 2, A and B). However, for ribosomes that lacked bL27, the amount of protein synthesized was lower at 15 and 30 min, consistent with published data (*23*). A previous study with mutant strains of *E. coli* also found that deleting bL27 interfered with ribosome assembly (*24*). However, composite agarose-polyacrylamide gels and sucrose gradient profiles did not detect an increased fraction of partially assembled ribosomes in the Δ*rpmA* sample (Fig. 2, C and D). Furthermore, translation initiation assays indicated that the fraction of ribosomes that can form an initiation complex (IC) is the same in purifications of wild-type and Δ*rpmA* samples (Fig. 2E), suggesting that the decreased rate of protein synthesis in these assays is due primarily to slower translation in the absence of bL27 and not an increase in misassembled ribosomes.

We next used molecular simulations to gain insights into how bL27 can affect tmRNA movement through the ribosome. For these simulations, we used an all-atom structure-based (SMOG) model (*32*) to simulate the movement of tmRNA-SmpB between the A and P sites. We specifically compare the dynamics when the bL27 N-terminal tail is present or absent to determine the extent to which the steric composition of the tail can affect the kinetics of tmRNA movement.

These simulations indicate that the presence of the tail reduces the accessibility of tmRNA to the P site, consistent with the in vitro and in vivo measurements. We simulated 150 independent events for each system and found that the dwell time of the tRNA-like domain (TLD) of tmRNA in the A site is increased by roughly twofold when the full-length bL27 protein is present (Fig. 3, A and B), which is comparable to the approximately fourfold difference in EC_{50} values (Fig. 1B). This delay may be understood as arising from steric interactions between the flexible N terminus and the TLD acceptor stem (Fig. 3, C and D). That is, the N-terminal sequence bL27 can impede the movement of the tmRNA, thereby delaying access to the P site (Fig. 3E). In contrast, simulations showed that the dynamics of tRNA is not affected by the N terminus of bL27 (Fig. 3, F and G). This differential effect on tmRNA relative to tRNA can be understood as arising from differences in the pathways that are accessed by the two molecules. Early in the transition between the A and P sites, tmRNA closely interacts with bL27 (fig. S4A), while tRNA accesses paths that are farther away (fig. S4B). Accordingly, accessing bL27-proximal paths (fig. S4C) allows bL27 to specifically affect the dynamics of tmRNA.

Together, these analyses suggest that the bL27 N terminus can act as a dynamic steric obstacle that transiently restricts tmRNA motion between the A and P sites. This provides a physical explanation for

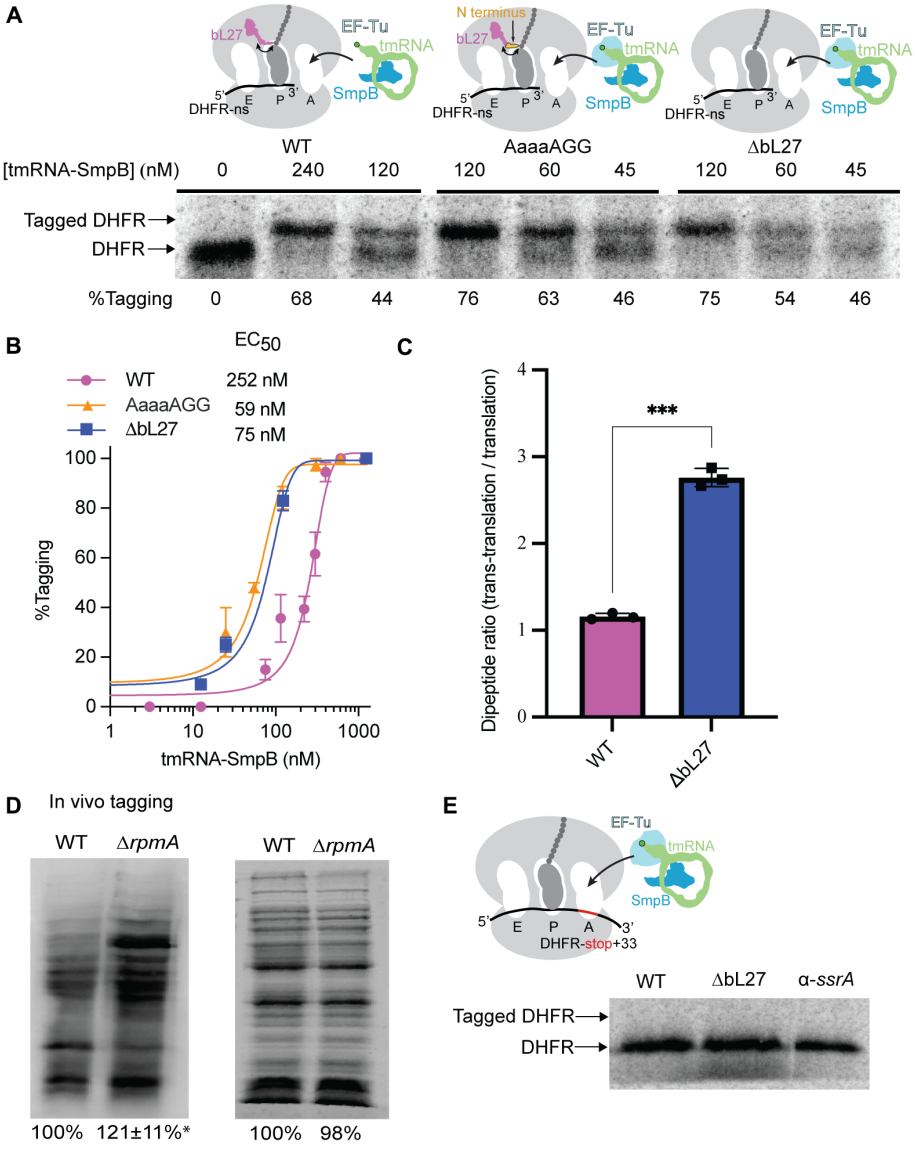

Fig. 1. Trans-translation activity is higher on bL27 mutant ribosomes. In vitro trans-translation assays were performed using a nonstop DHFR template and wild-type (WT), AaaaAGG, or ΔbL27 ribosomes, with varying concentrations of tmRNA-SmpB. (**A**) Gel image of a representative assay. The mobility of tagged and untagged DHFR is indicated with the percent tagging calculated after quantification of the tagged and untagged bands. (**B**) The average percent tagging from experiments as in (A) was plotted with whiskers indicating standard deviations. Averages were calculated from at least three trials at each concentration. The data were fit to a three-parameter sigmoid equation, and EC_{50} is shown. (**C**) The transfer of methionine from $tRNA^{fMet}$ to tmRNA or $tRNA^{Ala}$ in an in vitro system using wild-type or ΔbL27 ribosomes was monitored by electrophoretic thin-layer chromatography and quantified. The trans-translation end-point product was normalized to the translation end-point product from the same ribosomes ($n = 3$, $^{***}P = 0.0005$, Student's unpaired t test). (**D**) The amount of tagged proteins in wild-type and Δ*rpmA* cells expressing tmRNA-HHHHHHD was measured by Western blotting with an anti-his6 antibody. (Left) A representative Western blot is shown. The total signal was quantified and normalized to the wild type. Averages from three repeats are indicated with the standard deviation ($^{*}P = 0.04$, two-tailed one-sample Student's t test versus 100%). (Right) Coomassie-stained gel showing the amounts of total protein loaded for the Western blot analysis. (**E**) In vitro trans-translation assays were performed using the DHFR-stop+33 template and no RFs with wild-type or ΔbL27 ribosomes. A representative gel is shown, with arrows indicating the mobility of the tagged and untagged DHFR. A control reaction containing an α-SsrA oligo to eliminate trans-translation is included to confirm the mobility of untagged DHFR.

the biochemical observation that trans-translation activity is lower with wild-type ribosomes.

Deletion of *ssrA* rescues death phenotype in cells lacking bL27

Previous work with mutant *E. coli* strains has shown that bL27 is not essential, although cells grow slower in its absence (*24*, *25*). Using the wild-type strain MG1655, we found that deletion of bL27 leads to substantially slower growth because of two distinct effects (Fig. 4A). Plating assays showed that saturated cultures of Δ*rpmA* cells have a 10,000-fold decrease in colony-forming units (CFU) compared to the wild type, indicating that most of the Δ*rpmA* cells are dead (Fig. 4B). This decrease in CFU causes an extended lag phase compared to the wild type. Once the Δ*rpmA* cells enter exponential growth, they have

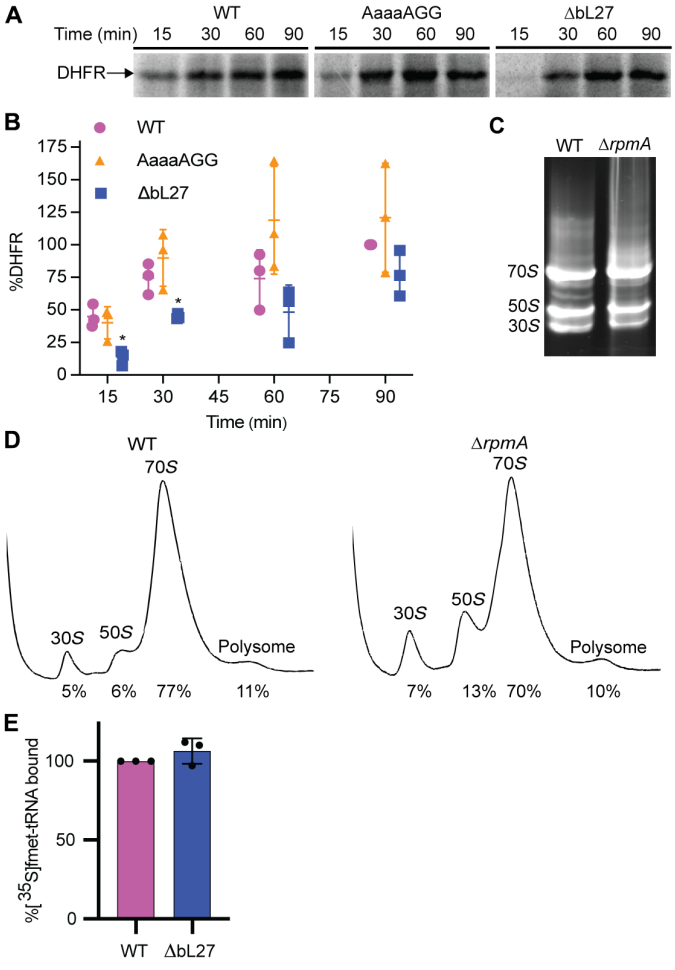

Fig. 2. Effects of bL27 mutations on translation. (**A**) In vitro translation reactions were performed with wild-type and mutant ribosomes. A representative gel image is shown with an arrow indicating the mobility of the DHFR product. (**B**) Gels as in (A) were quantified, and the amount of DHFR protein was normalized to the level produced by the wild type at 90 min and plotted with the means and standard deviation indicated ($n = 3$: $^*P \leq 0.0135$, two-tailed Student's t test versus wild type). (**C**) Cell lysates from the indicated strains were separated on agarose-polyacrylamide composite gels to visualize ribosomal subunits. A representative gel is shown, with the mobility of 70*S* ribosomes and 50*S* and 30*S* subunits indicated. (**D**) Sucrose density gradient profiles on cell lysates from the indicated strains. Peaks were quantified, and the percentage relative to total ribosomes is indicated. (**E**) The ability of purified ribosomes to form an IC was measured by incubating ribosomes with DHFR mRNA, initiation factors, $tRNA^{fMet}$, and [^{35}S]Met and quantifying radioactivity retained on nitrocellulose filters. The percentage of [^{35}S]Met-tRNA bound to ΔbL27 ribosomes was calculated relative to the wild type and is not significantly different ($n = 3$).

a slower doubling time than the wild type. Both phenotypes were largely complemented by the expression of bL27 from a multicopy plasmid (Fig. 4).

To determine whether trans-translation plays a role in the Δ*rpmA* growth defect, we deleted *ssrA* in the wild-type and Δ*rpmA* strains and measured growth parameters. Deletion of *ssrA* increases the CFU in Δ*rpmA* cells by 100-fold but has no detectable effect on the CFU for the wild type (Fig. 4B). In contrast, deletion of *ssrA* had little impact on the growth rate in the exponential phase. These results indicate that tmRNA is problematic in the absence of bL27 when cells are in the stationary phase but not during exponential growth.

bL27 limits tmRNA-SmpB interference with translation elongation

Why does tmRNA increase cell death in the absence of bL27? Our biochemical data can be explained by a model in which bL27 limits the interaction of tmRNA-SmpB with elongating ribosomes as well as nonstop ribosomes. In this scenario, the absence of bL27 could allow tmRNA-SmpB to interfere with the dynamics of translation elongation. To test this possibility, we performed in vitro translation assays in the presence and absence of tmRNA-SmpB. As expected, addition of tmRNA-SmpB to reactions with wild-type ribosomes had little effect (Fig. 5, A and B). However, with ΔbL27 ribosomes, addition of tmRNA-SmpB decreased the rate of protein production by up to 23% in a concentration-dependent manner (Fig. 5A). This result confirms that bL27 limits tmRNA-SmpB interference with translation.

DISCUSSION

Our biochemical and computational analyses provide two possible explanations for how tmRNA-SmpB association with the ribosome leads to this reduced rate of protein production. First, during elongation, tmRNA-SmpB may transiently interact with the A site of the ribosome, accommodating when there is no mRNA and dissociating when mRNA is present. In the absence of bL27, these transient events may be prolonged, reducing the rate of translation by sterically blocking tRNAs and RFs. Alternatively, the absence of bL27 may allow tmRNA to more easily access the PTC during elongation, which could allow for premature transpeptidation events. Our data show that trans-translation does not occur on elongating ribosomes, even in the absence of bL27, so transpeptidation to tmRNA would have to occur without the subsequent steps of trans-translation. Such inappropriate transpeptidation to tmRNA seems unlikely, but the size and flexibility of tmRNA suggest that it may be able to reach the PTC without SmpB binding in the empty mRNA channel, leading to inactive ribosomes instead of trans-translation. Further experiments will be required to determine the precise mechanism by which tmRNA-SmpB slows translation. Nevertheless, the data presented here indicate a central role for bL27 in limiting interference by tmRNA-SmpB with translation elongation (Fig. 5C).

Both bL27 and tmRNA-SmpB are conserved in the vast majority of bacterial species, and the N-terminal residues of bL27 are almost invariant (fig. S5). The functional interaction we observe here may account for this co-conservation. The absence of bL27 and tmRNA-SmpB from eukaryotes provides the opportunity to target this interaction with new broad-spectrum antibiotics.

MATERIALS AND METHODS

Bacterial strains, plasmids, and growth conditions

All strains (table S1) were grown at 37°C with shaking (250 rpm) in lysogeny broth (LB) supplemented with ampicillin (50 μg/ml), kanamycin (30 μg/ml), chloramphenicol (20 μg/ml), or 1 mM isopropyl-thio-β-D-galactoside as appropriate, unless otherwise described. To make the strain X90 *ssrA*6HisD Amp^R, *rpmA*::kan, *rpmA*::kan was moved from IW312 *rpmA*::kan (table S1) into X90 *ssrA*6HisD Amp^R

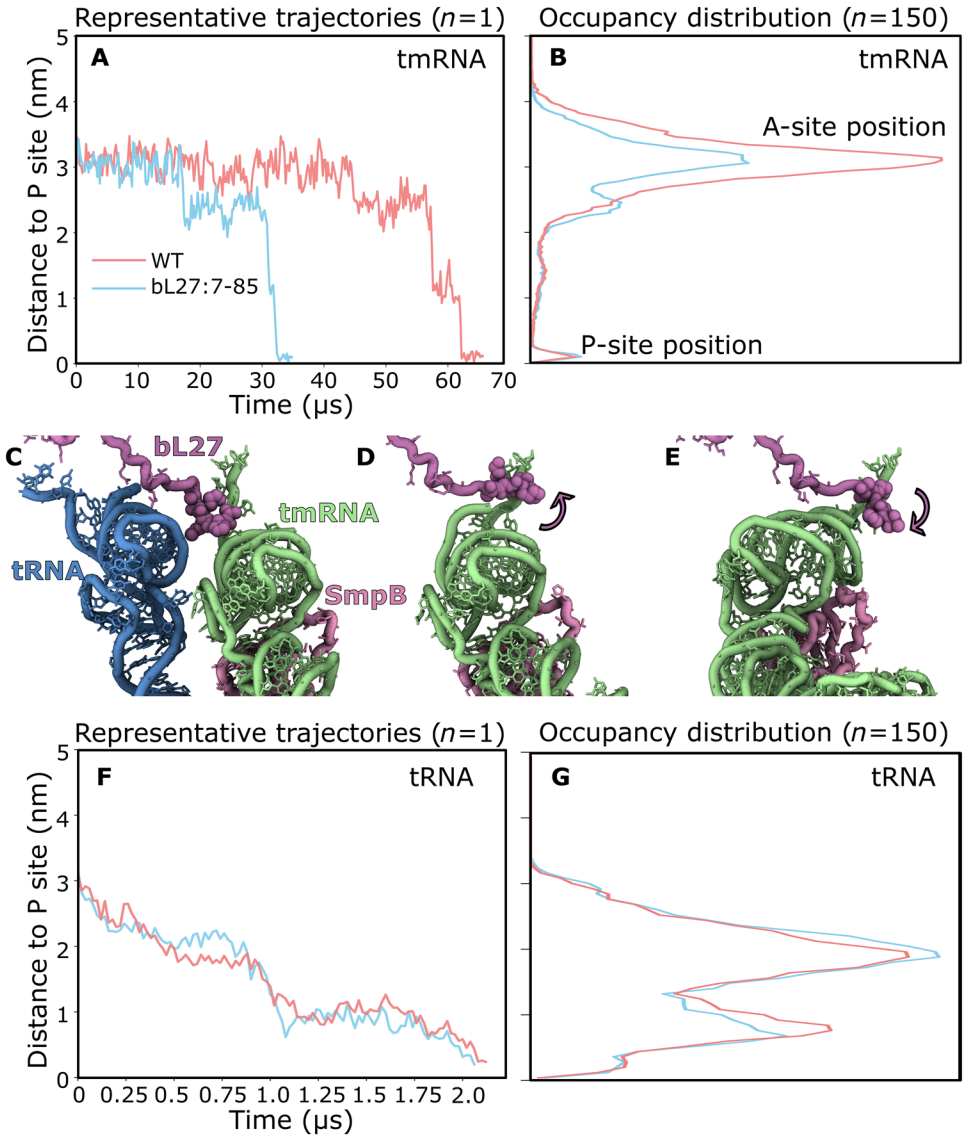

Fig. 3. bL27 slows the movement of tmRNA-SmpB during translocation. (**A**) Representative simulations of tmRNA-SmpB translocation with full-length (red) and truncated bL27 (blue) show that the N-terminal tail prolongs sampling of the ribosomal A site. The distance to the P site is defined as the distance of the P atom of U9 from its posttranslocation position on the LSU. (**B**) Occupancy of tmRNA position for the full-length and truncated systems, each calculated from 150 independent simulations. (**C**) Initially (distance ~3 nm), deacylated tRNA (blue) leaves the P site and the disordered tail of bL27 (purple) makes close contact with tmRNA (green). (**D**) During tmRNA movement toward the P site (distance ~2.2 nm), bL27 is sterically confined, which impedes the transition. (**E**) After tmRNA reaches the P site (distance ~0.1 nm), the bL27 tail can again adopt an extended disordered form. (**F**) Representative trajectories of tRNA for the wild type and truncated-bL27 model show similar kinetics. The distance to the P site was calculated on the basis of the P atoms of tRNA residue A9. (**G**) Distribution of tRNA conformations, calculated from 150 simulations. Distributions are similar, which shows that the effect of bL27 is specific to tmRNA translocation.

by P1 phage–mediated transduction. To delete *rpmA* in MG1655 *tolC*::cat, *rpmA*::kan was moved from IW312 *rpmA*::kan (table S1) into MG1655 *tolC*::cat (table S1) by P1 phage–mediated transduction. To delete *ssrA* in the Δ*rpmA* background, first, the CAT cassette was flipped out of MG1655 *tolC*::cat *rpmA*::kan with pCP20 (table S1), selected on plain LB plates, and grown at 40°C, resulting in MG1655 Δ*tolC rpmA*::kan. The *ssrA*::cat deletion from MG1655 *ssrA*::cat was moved into MG1655 Δ*tolC rpmA*::kan by phage-mediated transduction, resulting in MG1655 Δ*tolC rpmA*::kan *ssrA*::cat. *rpmA* mutations were introduced into the linearized pL27 plasmid via HiFi Assembly (NEB, Ipswich, MA) using a 60–base pair oligonucleotide (IDT, Coralville, IA) containing the mutations of interest (table S2) to make the 11 plasmids containing *rpmA* mutations (table S1). The 12 plasmids containing *rpmA* mutations including the one with wild-type *rpmA* (table S1) were then transformed separately into MG1655 *tolC*::cat *rpmA*::kan, resulting in strains expressing mutant bL27 in the *rpmA* deletion background (table S1). The plasmid pL27, pL27 AaaaAGG, or vector only was transformed into the *ssrA* deletion background strain (MG1655 Δ*tolC rpmA*::kan *ssrA*::cat) to express bL27 mutations in the *ssrA* deletion background (table S1).

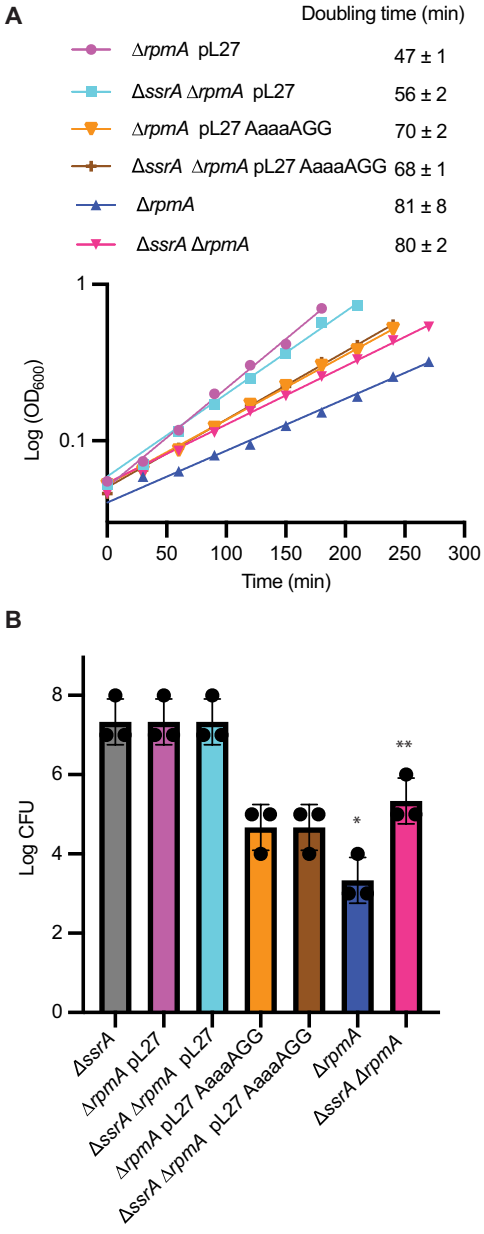

Fig. 4. Deletion of *ssrA* partially complements the growth defect of Δ*rpmA* strain in the stationary phase. (**A**) Growth curves of mutant strains monitored during exponential growth. The average doubling times (±standard deviation) from three experiments are shown. (**B**) The bar graph shows that log CFU determined by the spot plate method and deletion of *ssrA* in Δ*rpmA* strain had 100-fold higher CFU than Δ*rpmA* ($n = 3$ independent biological replicates; unpaired two-tailed Student's *t* test, $^*P = 0.25$ and $^{**}P = 0.26$ compared to Δ*ssrA*).

Growth rate measurements

The doubling times of all the strains were measured by optical density at 600 nm (OD_{600}) readings of each strain grown in 2 ml of LB with required supplements. Starting OD_{600} was set to 0.05 by inoculating from overnight cultures. Doubling times were calculated from the exponential phase ($OD_{600} = 0.1$ to 0.6), fitting the curves to the exponential growth curve function in GraphPad Prism (version 10.6, GraphPad Software LLC, San Diego, CA).

Spot plate assays

Overnight cultures were back-diluted to $OD_{600} = 0.05$ and grown for 48 hours. Cultures were serially diluted 10-fold in sterile LB medium. Aliquots (5 μl) of each dilution were spotted onto LB agar plates with the supplements, as needed. Plates were incubated at 37°C for 24 hours.

Growth inhibition measurements

Overnight cultures were diluted to $OD_{600} = 0.004$, added to twofold serial dilution concentrations of compounds or drugs in a 96-well plate, and grown at 37°C for 24 hours, and OD_{600} was measured using a SpectraMax plate reader (Molecular Devices, Sunnyvale, CA). The compound concentrations were plotted against normalized OD_{600} in Sigmaplot version 10, San Jose, CA, and fit with three-parameter sigmoidal function to obtain IC_{50} values. Averages of IC_{50} values with standard deviations and number of trials are indicated in fig. S1. Statistical significance was tested using a GraphPad Bonferroni multiple-comparisons analysis of variance (ANOVA) on selected pairs.

Purification of ribosomes for in vitro assays and sucrose density gradient profiles on lysates

Crude ribosomes were prepared as described previously (*33*). 70*S* ribosomes were isolated by sucrose density fractionation. Crude ribosome [200 μl of 50 absorbance at 260 nm (A_{260}) units] was loaded on a 10 to 40% linear gradient of sucrose in ribosome resuspension buffer [20 mM Hepes-KOH (pH 7.6), 60 mM NH_4Cl, 12 mM $MgCl_2$, 0.5 mM EDTA, and 6 mM β-mercaptoethanol (β-ME)] and centrifuged at 151,000*g* for 2.5 hours in a Beckman SW-41 rotor (Beckman Coulter, Brea, CA). Fractions containing 70*S* ribosomes were harvested by fractionation with the Piston Gradient Fractionator (Biocomp, Tatamagouche, NS, Canada), and fractions were pooled and centrifuged at 220,000*g* for 24 hours at 4°C. The 70*S* ribosomal pellet was resuspended and stored at −80°C in ribosome resuspension buffer. For sucrose density gradient profiles on lysates, cleared cell lysate (200 μl of 50 A_{260} units) was loaded on a 10 to 40% sucrose linear gradient, and fractionation was done as described above.

Isolation of tmRNA and purification of SmpB

E. coli tmRNA was transcribed in vitro as described previously (*15*). For purification of SmpB, *E. coli* BL21 (DE3) with pET28 *smpB* (table S1) were grown in terrific broth supplemented with kanamycin (50 μg/ml) at 37°C to $OD_{600} = 0.6$ and induced with 1 mM isopropyl-thio-β-D-galactoside for 3 hours. The cells were harvested by centrifugation at 6953*g* for 20 min, resuspended in lysis buffer/wash buffer [100 mM $Na_2H_2PO_4$ (pH 7.6), 150 mM KCl, 6 M GuHCl, and 10 mM imidazole], and lysed by sonication, and cell debris was removed by centrifugation at 28,000*g* for 20 min. Cleared lysate was incubated with HisPur Ni-NTA agarose resin (Thermo Fisher Scientific, Waltham, MA) for 1 hour at 4°C and washed four times with 40 ml of wash buffer, and bound protein was eluted with 10 ml of elution buffer [100 mM $Na_2H_2PO_4$ (pH 7.6), 300 mM KCl, 6 M GuHCl, and 1 M imidazole]. The eluate was dialyzed against buffer [50 mM Hepes-KOH (pH 7.6), 300 mM KCl, 10 mM $MgCl_2$, 20% (v/v) glycerol, and 7 mM β-ME] at 4°C.

In vitro trans-translation and translation

The *E. coli* in vitro transcription-translation system was designed on the basis of the OnePot PURE system (*34*). The energy solution was

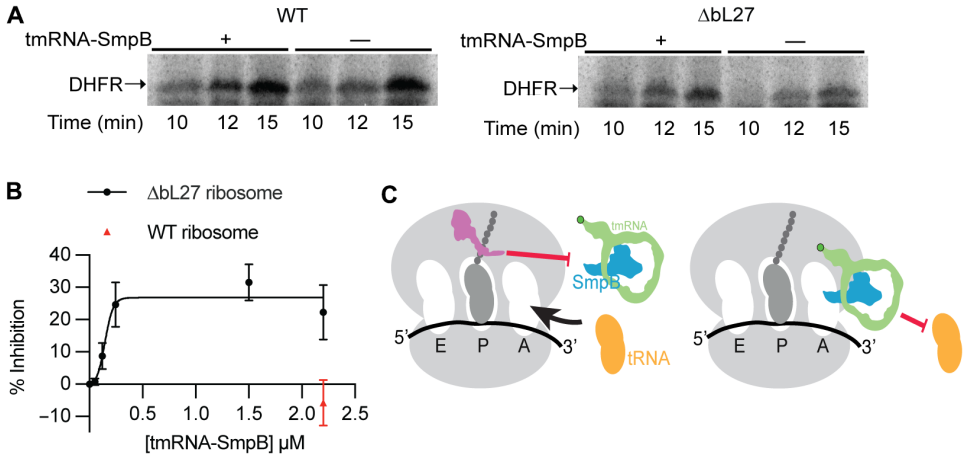

Fig. 5. tmRNA-SmpB slows protein synthesis in the absence of bL27. (**A**) In vitro translation reactions were performed using the DHFR-Stop+33 template in the presence or absence of tmRNA-SmpB with wild-type or ΔbL27 ribosomes. Representative gels are shown. (**B**) Assays as in (A) were repeated with varying concentrations of tmRNA-SmpB, and the average percentage decrease in rate compared to reactions with no tmRNA-SmpB is plotted with error bars indicating the standard deviation. (**C**) Model for the role of bL27 during elongation. bL27 limits the access of tmRNA-SmpB to the ribosome, allowing the rapid entry of tRNAs to the A site. In the absence of bL27, tmRNA-SmpB has a longer dwell time in the A site and limits the entry of tRNAs.

prepared as described previously (*34*). tRNAs for energy solution was purified from *E. coli* MRE 600, as described previously (*35*). A protein solution was made with proteins purified the same way as described previously but from strains listed in table S1 and was made without adding RFs (RF1, RF2, and RF3) and EF-Tu (*34*). An RF mix containing RF1, RF2, and RF3 was purified using strains listed in table S1, as described previously (*34*). EF-Tu was purified as described previously (*36*). A DNA template encoding DHFR gene without a stop codon (DHFR-ns), the DNA template DHFR with a stop codon (DHFR-stop), and a DNA template with DHFR with a stop codon and 33 nucleotides past the stop codon (DHFR-stop+33) were prepared via polymerase chain reaction, as described previously (*15*, *37*). In vitro trans-translation reactions were set up with the DHFR-ns template. The trans-translation reactions contained an energy solution (2 μl), protein solution (1 μl), EF-Tu (10 μM), 70*S* ribosomes (2.2 μM) (wild-type ribosomes, AaaaAGG mutant bL27 containing ribosomes, or ΔbL27 ribosomes), DHFR-ns DNA template (9 ng/μl), an RF mix (2.2 μM), [^{35}S]-methionine (0.42 μCi/μl), and varying equimolar concentrations of tmRNA and SmpB. The control reaction was set up the same way but with no tmRNA and smpB, and to inhibit any background trans-translation activity, 0.5 μM α-*ssrA* oligonucleotide was added (table S2). The reactions were incubated at 37°C for 90 min, acetone precipitated, boiled at 95°C for 10 min with 2× sample loading buffer (2% SDS; 20% glycerol; 0.004% bromophenol blue; 0.125 M tris-Cl, pH 6.8; and 6 mM β-ME), analyzed by SDS–polyacrylamide gel electrophoresis, and visualized by phosphor imaging (GE Healthcare, Chicago, IL). The band intensities of tagged DHFR-ns (higher molecular weight due to addition of the SsrA tag) and untagged DHFR-ns were quantified using ImageJ. % Trans-translation was calculated using the equation [tagged DHFR-ns/(DHFR-ns tagged + DFHR-ns untagged)]. [tmRNA-SmpB] added to the trans-translation reactions was plotted against % tagging, and EC_{50} was calculated in Sigmaplot version 10.

In vitro translation experiments were set up with the following modifications to the trans-translation assay. Translation was tested on the DHFR-stop DNA template. 4X reaction was set up and incubated at 37°C, and samples were taken out at 15, 30, 60, and 90 min, acetone precipitated, and analyzed by SDS–polyacrylamide gel electrophoresis, as described above. The band intensity of DHFR-stop was quantified. Relative % DHFR formed at each time point was calculated using the equation (DHFR-stop intensity/DHFR-stop intensity with wild-type ribosomes at 90 min).

To assess the competition of tmRNA and tRNA with or without bL27, in vitro translation reactions were set up with the DHFR-stop+33 DNA template as described above with following modifications. The translation reactions were set up with varying tmRNA-SmpB concentrations (0, 0.05, 0.120, 0.245, 1.5, and 2.2 μM) and incubated at 30°C, and samples were withdrawn at 10, 12, and 15 min for analysis. The intensity of the DHFR band was quantified and plotted against time, and the rate of translation was calculated from the slope of the plots. The percentage change in the rate of translation was calculated as a percentage relative to the rate of translation without tmRNA-SmpB.

Reconstituted in vitro translation assay for peptidyl transfer

A reconstituted in vitro translation assay was used to measure the amount of ^{f}Met-Ala dipeptide formed with tRNA or tmRNA in ribosome complexes with and without bL27. The ribosomes were purified as mentioned above. *E. coli* initiation factors, elongation factors, total tRNA, and tRNA^{fMet} were purified as previously described (*38*).

Aminoacylated *E. coli* initiator tRNA^{fMet} (fMet-tRNA^{fMet}) was made with [^{35}S]-methionine described previously (*39*), with minor modifications. Reactions were assembled in aminoacylation buffer (10 mM Hepes-KOH, pH 7.5; 2 mM KCl; and 4 mM $MgCl_2$) supplemented with 2 mM dithiothreitol, 3 mM adenosine 5′-triphosphate (pH 7), 300 μM neutralized N^{10}-formyl-tetrahydrofolate (Sigma-Aldrich), 5 μM tRNA^{fMet}, 38 μM L-methionine, [^{35}S]-methionine, 1 μM methionyl-tRNA formyltransferase, and 1 μM methionyl-tRNA synthetase. Reactions were incubated at 37°C for 30 min. Aminoacylated tRNA was extracted with an equal volume of acidic phenol:chloroform:isoamyl alcohol (25:24:1, pH 4.5), vortexed for 30 s, and centrifuged at 16,000*g* for 5 min at 4°C. The aqueous layer was reextracted once and then desalted using an Econo-Pac 10DG Desalting Column (Bio-Rad) pre-equilibrated with 300 mM NaOAc, pH 5.2. Eluted fractions were pooled, ethanol precipitated, and resuspended in 20 mM KOAc

(pH 4.8). The concentration of ^{35}S-fMet-tRNA^{fMet} was determined by scintillation counting. Aliquots were stored at −80°C.

Aminoacylation of tmRNA and total tRNA was performed similarly to the fMet-tRNA^{fMet} procedure with some modifications. Briefly, reactions were assembled in aminoacylation buffer supplemented with 1 mM dithiothreitol, 10 mM adenosine 5′-triphosphate, 100 μM L-alanine, 4.5 μM tmRNA or total tRNA, and 75 μM alanyl-tRNA synthetase. Reactions were incubated at 37°C for 30 min. Aminoacylated tmRNA and tRNA were purified and stored as described for fMet-tRNA^{fMet}, except that the final concentration was determined by A_{260}.

ICs were assembled by combining translation buffer (50 mM Hepes-KOH, pH 7.6; 70 mM NH_4Cl; 30 mM KCl; 7 mM $MgCl_2$; and 5 mM β-ME); 1 mM guanosine 5′-triphosphate (GTP); initiation factors IF1, IF2, and IF3 (2 μM each); 2 μM mRNA; 1 μM 70*S* ribosomes; and 2 μM ^{35}S-fMet-tRNA^{fMet}. Two mRNA constructs were used: a canonical message (5′-GGC AAG GAG GUA AAA AUG GCC-3′) and a nonstop (5′-GGC AAG GAG GUA AAA AUG-3′), synthesized by IDT. For trans-translation reactions, a nonstop mRNA was used. Reactions were incubated at 37°C for 30 min. ICs were then layered onto a cold sucrose cushion (20 mM tris-Cl, pH 7.5; 500 mM NH_4Cl; 0.5 mM EDTA; 10 mM $MgCl_2$; and 1.1 M sucrose) and spun at 69,000 rpm for 2 hours at 4°C using a TLA-120.1. After centrifugation, the supernatant was carefully removed, and the pellet containing the 70*S* ICs was resuspended in translation buffer and stored at −80°C.

Ternary complexes (EF-Tu•GTP•aminoacyl-tRNA) or quaternary complexes (EF-Tu•GTP•Ala-tmRNA•SmpB) were formed as follows. EF-Tu (80 μM) was preincubated with 5 mM GTP in translation buffer at 37°C for 15 min. In parallel, aminoacylated total tRNA or tmRNA-SmpB was incubated in translation buffer containing 5 mM GTP and kept on ice. EF-Tu•GTP was then added to aminoacylated tRNA or tmRNA-SmpB mixtures and incubated at 37°C for 10 min to allow complex formation.

An IC and ternary complex were mixed in equal volumes and incubated at 37°C. Samples were taken at respective time points and treated with an equal volume of 1 M KOH to hydrolyze peptidyl-tRNA. Dipeptide formation was resolved by electrophoretic thin-layer chromatography at 1200 V for 30 min (*38*). Plates were exposed to a phosphor screen and imaged using a Typhoon scanner (Cytiva, Marlborough, MA). Band intensities were quantified using ImageQuant TL analysis software (Cytiva, Marlborough, MA).

In vivo trans-translation tagging with or without bL27

To assess total in vivo tagging in strains with or without bL27, X90 *ssrA*6HisD and X90 *ssrA*6HisD *rpmA*::kan (table S1) were grown to an OD_{600} of 0.6, harvested by centrifugation, and weighed. Pellets were resuspended in 2× sample loading buffer in proportion to wet cell mass and heated at 95°C for 5 min. Western blotting was performed with a Penta-His antibody (Qiagen, Hilden, Germany, 1:10,000 dilution) followed by a goat anti-mouse IgG-alkaline phosphatase conjugate (Sigma-Aldrich, St. Louis, MO, 1:20,000 dilution). Signals were detected using the ECF substrate (Cytiva, Amersham, Marlborough, MA) and visualized with the ChemiDoc imaging system (Bio-Rad, Hercules, CA).

Translation initiation assay

An energy solution for translation initiation reaction was prepared as described previously with modifications (*34*). The energy solution included only methionine instead of all 20 amino acids, and tRNAs were not added. A modified protein solution was prepared by purifying proteins as described previously, but the modified protein solution contained proteins that are only required for translation initiation (creatine kinase, myokinase, nucleoside-diphosphate kinase, methionyl-tRNA transformylase, IF1, IF2, and IF3). DHFR-stop mRNA was in vitro transcribed as described previously (*34*). Met tRNA was in vitro transcribed as described previously with the metZ DNA template with a T7 promoter (*15*). The metZ DNA template for in vitro transcription was amplified from *E. coli* genomic DNA using primer pairs listed in table S2. In vitro translation initiation reactions were set up with 1 μl of modified energy solution, 0.8 μl of modified protein solution, 70*S* ribosomes (2 μM), DHFR-stop mRNA (2.5 μM), [^{35}S]-methionine (0.42 μCi/μl), and tRNA^{met} (2.5 μM). The reactions were incubated for 15 min at 37°C. The reaction mix was passed under vacuum through 0.45-μm nitrocellulose membrane filter (MilliporeSigma, Burlington, MA) presoaked with wash buffer [20 mM Hepes-KOH (pH 7.6), 60 mM NH_4Cl, 12 mM $MgCl_2$, and bovine albumin serum (50 μg/ml)]. The membranes were washed and dried, and radioactivity retained on the membrane was determined by scintillation counting.

Agarose-polyacrylamide composite gel electrophoresis

Cells were grown to OD_{600} = 0.6 and lysed by sonication with buffers described previously (*33*). The lysate was cleared by centrifugation at 28,000*g* for 30 min at 4°C. Ribosome complexes were analyzed using agarose-polyacrylamide composite gels prepared in tris/borate/MgOAc (TBM) buffer. Gels containing 1% agarose and 6% acrylamide (19:1) were prerun for 60 min at 100 V in 1× TBM at 4°C. Cleared lysates (10 A_{260} units) were mixed with loading buffer (20% sucrose, 1× TBM, and bromophenol blue) and resolved at 100 V for 180 min at 4°C. Gels were stained with ethidium bromide (25 μg/ml) and visualized with ultraviolet illumination.

Molecular dynamics simulations

To investigate the potential impact of steric interactions between bL27 and the TLD of tmRNA, we used a structure-based force field ("SMOG") of the tmRNA-SmpB-ribosome complex (*40*). In this approach, all tmRNA-SmpB interactions with the ribosome that are present in the posttranslocation configuration [Protein Data Bank (PDB) ID: 7ACJ (*6*)] were explicitly defined as stabilizing, while intraribosomal contacts were defined to stabilize the pretranslocation conformation [PDB ID: 7AC7 (*6*)]. Non-native interactions were assigned repulsive potentials, which ensures that only sterically accessible conformations are sampled in the simulations. Given that the stabilizing interactions are defined on the basis of the end points (i.e., tmRNA in the A and P sites), this force field is suited to capture steric and entropic contributions to the dynamics (*32*, *41*, *42*). For example, these models have shown how tRNA dynamics is regulated by steric factors during P/E hybrid formation and translocation of tRNA (*43*–*45*). Here, to isolate the contributions of the bL27 N-terminal sequence, two sets of simulations were performed. In the first set, the bL27 N-terminal residues (Ala^2-Ala^6) were included and treated as disordered, consistent with the frequent lack of density for this region (PDB ID: 7ACJ). In the second set of simulations, we used an identical model, except that the N-terminal residues were removed (bL27:7-85). To investigate the effects of bL27 on tRNA during translocation, we used the same strategy, in which the tRNA posttranslocated state on the ribosomal large subunit

(LSU) [PDB ID: 7K51 (*46*)] was defined as the stable end point, and simulations were initiated from the pretranslocated conformation [PDB ID: 7K50 (*46*)].

Potential energy function

An all-atom structure-based (SMOG) force field of the tmRNA-SmpB-ribosome complex was used. The potential energy may be expressed as

$$U = \sum_{\text{bonds}} \frac{\epsilon_r}{2}(r_i - r_{i,0})^2 + \sum_{\text{angles}} \frac{\epsilon_\theta}{2}(\theta_i - \theta_{i,0})^2 + \sum_{\text{impropers}} \frac{\epsilon_{\chi_{imp}}}{2}(\chi_i - \chi_{i,0})^2 + \sum_{\text{planars}} \frac{\epsilon_{\text{planar}}}{2}\cos(2\chi_i - \pi)$$
$$+ \sum_{\text{backbone dihedrals}} \epsilon_{bb} F(\phi_i - \phi_{i,0}) + \sum_{\text{sidechain dihedrals}} \epsilon_{sc} F(\phi_i - \phi_{i,0})$$
$$+ \sum_{\text{intracontacts}} \epsilon_c \left[\left(\frac{\sigma_{ij}}{r_{ij}}\right)^{12} - 2\left(\frac{\sigma_{ij}}{r_{ij}}\right)^{6} \right] + \sum_{\text{intercontacts}} \frac{\epsilon_c}{3} \left[\left(\frac{\sigma_{ij}}{r_{ij}}\right)^{12} - 4\left(\frac{\sigma_{ij}}{r_{ij}}\right)^{3} \right]$$
$$+ \sum_{\text{noncontacts}} \left(\frac{C_{18}}{r_{ij}^{18}} - \frac{C_{12}}{r_{ij}^{12}} \right)$$

where

$$F(\phi) = \left[1 - \cos(\phi)\right] + \frac{1}{2}\left[1 - \cos(3\phi)\right]$$

$\{r_0\}$ and $\{\theta_0\}$ parameters are assigned according to the Amber99sb-ildn force field (*47*), whereas the dihedral parameters ($\{\chi_0\}$ and $\{\phi_0\}$) are given the corresponding values found in the experimental model. The energetic weights are $\epsilon_r = 100\ \frac{\epsilon}{\text{Å}^2}$, $\epsilon_\theta = 80\ \frac{\epsilon}{\text{rad}^2}$, $\epsilon_{\chi_{\text{imp}}} = 10\ \frac{\epsilon}{\text{rad}^2}$, and $\epsilon_{\chi_{\text{planar}}} = 40\ \frac{\epsilon}{\text{rad}^2}$, where ϵ denotes the reduced energy unit. Nonbonded contacts found in the experimental model are identified using the Shadow Contact Map algorithm (*48*), with a shadowing radius of 1 Å and a cutoff distance of 6 Å. Intramolecular contacts within the ribosome and the tmRNA-SmpB complex were modeled using an attractive 6-12 potential to stabilize a preassigned structure. The intraribosomal contacts and dihedrals were assigned to stabilize the pretranslocation structure (PDB ID: 7AC7), while the intra–tmRNA-SmpB complex contacts and dihedrals were defined on the basis of the translocated structure (PDB ID: 7ACJ). To define the contacts between the ribosome and tmRNA-SmpB, long-range interactions were modeled with a 3-12 potential with the minimum assigned from the translocated configuration.

Given that contact terms in the structure-based model describe effective interactions (*49*), subsets of the contact weights were rescaled. Contacts between the head and body of the 30*S* ribosomal subunit and between the head of the 30*S* and the large subunit were rescaled by a factor of 0.5 to allow for the head rotation and tilting (*50*), while interactions between the A-site finger and 30*S* were rescaled by 0.2 to allow for the A-site finger to move toward its posttranslocation position. Intercomplex contacts between tmRNA-SmpB and the ribosome were rescaled by a factor of 0.6 to account for the transient nature of tmRNA-SmpB binding to the ribosome.

Atom pairs not in native contact in the experimental structure were assigned a purely repulsive interaction to represent excluded-volume effects using the 12-18 potential. The weights of dihedral and contact energies were normalized following the procedure described previously (*51*).

In these simulations, we additionally introduced a harmonic potential (weight of $2\ \frac{\epsilon}{\text{Å}^2}$) between the 3′-CCA tail of the tmRNA and the P site of the LSU. Specifically, the restraint was introduced between the phosphate atoms of A363 in the tmRNA and C2064 in the LSU. This was introduced to mimic a post–peptidyl transfer state, where the CCA end is chemically bonded to the nascent protein chain. Accordingly, our model is suited to address the impacts of bL27 on translocation of tmRNA-SmpB, rather than probe the direct impact on transpeptidation.

In addition, for the tRNA translocation simulations, all intramolecular contacts and dihedrals for the ribosome and tRNA were assigned values, stabilizing the translocated conformation (PDB ID: 7K51), using a 6-12 potential for native contacts. Intermolecular ribosome-tRNA interactions were modeled using a 3-12 potential, with contact strengths rescaled by a factor of 0.6 to reflect the transient nature of tRNA-ribosome interactions during translocation. To ensure the robustness of the results, simulations were repeated for tRNA, where the 3-12 contacts were scaled by 0.3. For both sets of parameters, the dynamics of tRNA were insensitive to the tail of bL27. Moreover, to mimic a post–peptidyl transfer state, a harmonic restraint with a weight of $2\ \frac{\epsilon}{\text{Å}^2}$ was introduced between A76 of the tRNA 3′-CCA tail and C2064 of the LSU.

Simulation details

All force field files were generated using the SMOG 2 (*40*) software package. The AA_12–18_Wang22.v1 templates (*52*) were used with SMOG 2 to generate the initial force field files, and manual modifications were introduced to include the 3-12 potential. Molecular dynamics simulations were performed using the OpenMM (*53*) and OpenSMOG (*54*) libraries. The system was simulated at a reduced temperature of $0.5\ \frac{\epsilon}{K_B}$, which was maintained using Langevin dynamics protocols with a time step of 0.002. This temperature was chosen because it yields predictions of molecular flexibility that are consistent with explicit-solvent simulations and crystallographic *B*-factors for molecular assemblies (*55*). To estimate the effective simulated time, we defined one reduced time unit to correspond to ~1 ns, as estimated for tRNA motion within the ribosome (*56*). This estimate was based on diffusion coefficients calculated from simulations using both SMOG and explicit-solvent models.

In preliminary simulations with our model, it was observed that the TLD always reached the P site before the mRNA-like domain. In addition, as sterically required, the deacylated tRNA was always displaced from the P site before TLD movement to the P site. To probe the effects of bL27, we focused the current analysis on the movement of the TLD.

Two sets of simulations with tmRNA were performed, each consisting of 150 independent runs: one with the complete bL27 N-terminal tail and the other with a truncated variant lacking residues Ala^2-Ala^6 (bL27:7-85). Each simulation was continued for up to 3.2×10^8 time steps. Simulations were continued until the TLD associated with the P site. For the full-length system, the TLD reached the P site in 112 simulations within the simulated time, while there were 130 successful events for the bL27:7-85 system. All 150 trajectories were used to calculate each occupancy distribution. Accordingly, the total occupancy values for the A-site occupancy represent lower-bound estimates. However, given that there were a larger number of simulations of the full-length system in which the tmRNA did not reach the P site, the A-site occupancy will likely increase more for the system with full-length bL27, which would further amplify the differences described in the main text.

Moreover, for the tRNA simulations, two sets of 150 independent replicas were performed, following the same protocol as in the tmRNA system. Simulations were terminated once the tRNA reached the P site of the LSU.

Supplementary Materials

This PDF file includes:

Figs. S1 to S5
Tables S1 and S2
References

REFERENCES

1. K. C. Keiler, Biology of *trans*-translation. *Annu. Rev. Microbiol.* **62**, 133–151 (2008).
2. S. D. Moore, R. T. Sauer, The tmRNA system for translational surveillance and ribosome rescue. *Annu. Rev. Biochem.* **76**, 101–124 (2007).
3. K. C. Keiler, N. S. Ramadoss, Bifunctional transfer-messenger RNA. *Biochimie* **93**, 1993–1997 (2011).
4. D. Camenares, D. P. Dulebohn, A. Svetlanov, A. W. Karzai, Active and accurate trans-translation requires distinct determinants in the C-terminal tail of SmpB protein and the mRNA-like domain of transfer messenger RNA (tmRNA). *J. Biol. Chem.* **288**, 30527–30542 (2013).
5. M. R. Miller, Z. Liu, D. J. Cazier, G. M. Gebhard, S. R. Herron, H. S. Zaher, R. Green, A. R. Buskirk, The role of SmpB and the ribosomal decoding center in licensing tmRNA entry into stalled ribosomes. *RNA* **17**, 1727–1736 (2011).
6. C. Guyomar, G. D'Urso, S. Chat, E. Giudice, R. Gillet, Structures of tmRNA and SmpB as they transit through the ribosome. *Nat. Commun.* **12**, 4909 (2021).
7. C. D. Rae, Y. Gordiyenko, V. Ramakrishnan, How a circularized tmRNA moves through the ribosome. *Science* **363**, 740–744 (2019).
8. K. C. Keiler, P. R. H. Waller, R. T. Sauer, Role of a peptide tagging system in degradation of proteins synthesized from damaged messenger RNA. *Science* **271**, 990–993 (1996).
9. J. M. Flynn, I. Levchenko, M. Seidel, S. H. Wickner, R. T. Sauer, T. A. Baker, Overlapping recognition determinants within the ssrA degradation tag allow modulation of proteolysis. *Proc. Natl. Acad. Sci. U.S.A.* **98**, 10584–10589 (2001).
10. S. Gottesman, E. Roche, Y. Zhou, R. T. Sauer, The ClpXP and ClpAP proteases degrade proteins with carboxy-terminal peptide tails added by the SsrA-tagging system. *Genes Dev.* **12**, 1338–1347 (1998).
11. J. S. Choy, L. L. Aung, A. W. Karzai, Lon protease degrades transfer-messenger RNA-tagged proteins. *J. Bacteriol.* **189**, 6564–6571 (2007).
12. K. C. Keiler, Mechanisms of ribosome rescue in bacteria. *Nat. Rev. Microbiol.* **13**, 285–297 (2015).
13. K. C. Keiler, H. A. Feaga, Resolving nonstop translation complexes is a matter of life or death. *J. Bacteriol.* **196**, 2123–2130 (2014).
14. Z. D. Aron, A. Mehrani, E. D. Hoffer, K. L. Connolly, P. Srinivas, M. C. Torhan, J. N. Alumasa, M. Cabrera, D. Hosangadi, J. S. Barbor, S. C. Cardinale, S. M. Kwasny, L. R. Morin, M. M. Butler, T. J. Opperman, T. L. Bowlin, A. Jerse, S. M. Stagg, C. M. Dunham, K. C. Keiler, trans-Translation inhibitors bind to a novel site on the ribosome and clear *Neisseria gonorrhoeae* in vivo. *Nat. Commun.* **12**, 1799 (2021).
15. N. S. Ramadoss, J. N. Alumasa, L. Cheng, Y. Wang, S. Li, B. S. Chambers, H. Chang, A. K. Chatterjee, A. Brinker, I. H. Engels, K. C. Keiler, Small molecule inhibitors of *trans*-translation have broad-spectrum antibiotic activity. *Proc. Natl. Acad. Sci. U.S.A.* **110**, 10282–10287 (2013).
16. M. Selmer, C. M. Dunham, F. V. Murphy IV, A. Weixlbaumer, S. Petry, A. C. Kelley, J. R. Weir, V. Ramakrishnan, Structure of the 70 *S* ribosome complexed with mRNA and tRNA. *Science* **313**, 1935–1942 (2006).
17. R. M. Voorhees, A. Weixlbaumer, D. Loakes, A. C. Kelley, V. Ramakrishnan, Insights into substrate stabilization from snapshots of the peptidyl transferase center of the intact 70S ribosome. *Nat. Struct. Mol. Biol.* **16**, 528–533 (2009).
18. P. Srinivas, K. C. Keiler, C. M. Dunham, Druggable differences: Targeting mechanistic differences between *trans*-translation and translation for selective antibiotic action. *Bioessays* **44**, e2200046 (2022).
19. Y. S. Polikanov, T. A. Steitz, C. A. Innis, A proton wire to couple aminoacyl-tRNA accommodation and peptide-bond formation on the ribosome. *Nat. Struct. Mol. Biol.* **21**, 787–793 (2014).
20. Y. Wang, M. Xiao, Role of the ribosomal protein L27 revealed by single-molecule FRET study. *Protein Sci.* **21**, 1696–1704 (2012).
21. M. Xiao, Y. Wang, L27–tRNA interaction revealed by mutagenesis and pH titration. *Biophys. Chem.* **167**, 8–15 (2012).
22. S. Trobro, J. Åqvist, Role of ribosomal protein L27 in peptidyl transfer. *Biochemistry* **47**, 4898–4906 (2008).
23. C. Maracci, I. Wohlgemuth, M. V. Rodnina, Activities of the peptidyl transferase center of ribosomes lacking protein L27. *RNA* **21**, 2047–2052 (2015).
24. I. K. Wower, J. Wower, R. A. Zimmermann, Ribosomal protein L27 participates in both 50 S subunit assembly and the peptidyl transferase reaction. *J. Biol. Chem.* **273**, 19847–19852 (1998).
25. B. A. Maguire, A. D. Beniaminov, H. Ramu, A. S. Mankin, R. A. Zimmermann, A protein component at the heart of an RNA machine: The importance of protein L27 for the function of the bacterial ribosome. *Mol. Cell* **20**, 427–435 (2005).
26. R. H. Connamacher, H. G. Mandel, Binding of tetracycline to the 30S ribosomes and to polyuridylic acid. *Biochem. Biophys. Res. Commun.* **20**, 98–103 (1965).
27. D. N. Wilson, F. Schluenzen, J. M. Harms, A. L. Starosta, S. R. Connell, P. Fucini, The oxazolidinone antibiotics perturb the ribosomal peptidyl-transferase center and effect tRNA positioning. *Proc. Natl. Acad. Sci. U.S.A.* **105**, 13339–13344 (2008).
28. J. R. Colca, W. G. McDonald, D. J. Waldon, L. M. Thomasco, R. C. Gadwood, E. T. Lund, G. S. Cavey, W. R. Mathews, L. D. Adams, E. T. Cecil, J. D. Pearson, J. H. Bock, J. E. Mott, D. L. Shinabarger, L. Xiong, A. S. Mankin, Cross-linking in the living cell locates the site of action of oxazolidinone antibiotics. *J. Biol. Chem.* **278**, 21972–21979 (2003).
29. C. S. Hayes, B. Bose, R. T. Sauer, Proline residues at the C terminus of nascent chains induce SsrA tagging during translation termination. *J. Biol. Chem.* **277**, 33825–33832 (2002).
30. N. Ivanova, M. Y. Pavlov, B. Felden, M. Ehrenberg, Ribosome rescue by tmRNA requires truncated mRNAs. *J. Mol. Biol.* **338**, 33–41 (2004).
31. C. Neubauer, R. Gillet, A. C. Kelley, V. Ramakrishnan, Decoding in the absence of a codon by tmRNA and SmpB in the ribosome. *Science* **335**, 1366–1369 (2012).
32. P. C. Whitford, J. N. Onuchic, Simulating biomolecules for physiological timescales. *Curr. Opin. Struct. Biol.* **92**, 103039 (2025).
33. A. Varshney, Z. Jia, M. D. Howe, K. C. Keiler, A. D. Baughn, A trans-translation inhibitor is potentiated by zinc and kills *Mycobacterium tuberculosis* and nontuberculous mycobacteria. *ACS Infect. Dis.* **11**, 1140–1152 (2025).
34. B. Lavickova, S. J. Maerkl, A simple, robust, and low-cost method to produce the PURE cell-free system. *ACS Synth. Biol.* **8**, 455–462 (2019).
35. G. Zubay, The isolation and fractionation of soluble ribonucleic acid. *J. Mol. Biol.* **4**, 347–356 (1962).
36. N. Marathe, H. A. Nguyen, J. N. Alumasa, A. B. Kuzmishin Nagy, M. Vazquez, C. M. Dunham, K. C. Keiler, Antibiotic that inhibits *trans*-translation blocks binding of EF-Tu to tmRNA but not to tRNA. *MBio* **14**, e01461–e01423 (2023).
37. H. A. Feaga, M. D. Quickel, P. A. Hankey-Giblin, K. C. Keiler, Human cells require non-stop ribosome rescue activity in mitochondria. *PLOS Genet.* **12**, e1005964 (2016).
38. J. G. Monroe, T. J. Smith, K. S. Koutmou, Investigating the consequences of mRNA modifications on protein synthesis using in vitro translation assays. *Methods Enzymol.* **658**, 379–406 (2021).
39. S. E. Walker, K. Fredrick, Preparation and evaluation of acylated tRNAs. *Methods* **44**, 81–86 (2008).
40. J. K. Noel, M. Levi, M. Raghunathan, H. Lammert, R. L. Hayes, J. N. Onuchic, P. C. Whitford, SMOG 2: A versatile software package for generating structure-based models. *PLoS Comput. Biol.* **12**, e1004794 (2016).
41. M. Levi, J. K. Noel, P. C. Whitford, Studying ribosome dynamics with simplified models. *Methods* **162-163**, 128–140 (2019).
42. A. Hassan, S. Byju, P. C. Whitford, The energetics of subunit rotation in the ribosome. *Biophys. Rev.* **13**, 1029–1037 (2021).
43. K. Nguyen, P. C. Whitford, Capturing transition states for tRNA hybrid-state formation in the ribosome. *J. Phys. Chem. B* **120**, 8768–8775 (2016).
44. M. Levi, K. Walak, A. Wang, U. Mohanty, P. C. Whitford, A steric gate controls P/E hybrid-state formation of tRNA on the ribosome. *Nat. Commun.* **11**, 5706 (2020).
45. K. Nguyen, P. C. Whitford, Steric interactions lead to collective tilting motion in the ribosome during mRNA–tRNA translocation. *Nat. Commun.* **7**, 10586 (2016).
46. G. Demo, H. B. Gamper, A. B. Loveland, I. Masuda, C. E. Carbone, E. Svidritskiy, Y.-M. Hou, A. A. Korostelev, Structural basis for +1 ribosomal frameshifting during EF-G-catalyzed translocation. *Nat. Commun.* **12**, 4644 (2021).
47. K. Lindorff-Larsen, S. Piana, K. Palmo, P. Maragakis, J. L. Klepeis, R. O. Dror, D. E. Shaw, Improved side-chain torsion potentials for the Amber ff99SB protein force field. *Proteins Struct. Funct. Bioinforma.* **78**, 1950–1958 (2010).
48. J. K. Noel, P. C. Whitford, J. N. Onuchic, The shadow map: A general contact definition for capturing the dynamics of biomolecular folding and function. *J. Phys. Chem. B* **116**, 8692–8702 (2012).
49. L. Huynh, C. Neale, R. Pomès, H. S. Chan, Molecular recognition and packing frustration in a helical protein. *PLoS Comput. Biol.* **13**, e1005909 (2017).
50. A. Hassan, S. Byju, F. C. Freitas, C. Roc, N. Pender, K. Nguyen, E. M. Kimbrough, J. M. Mattingly, R. L. Gonzalez Jr., R. J. de Oliveira, C. M. Dunham, P. C. Whitford, Ratchet, swivel, tilt and roll: A complete description of subunit rotation in the ribosome. *Nucleic Acids Res.* **51**, 919–934 (2023).
51. P. C. Whitford, J. K. Noel, S. Gosavi, A. Schug, K. Y. Sanbonmatsu, J. N. Onuchic, An all-atom structure-based potential for proteins: Bridging minimal models with all-atom empirical forcefields. *Proteins Struct. Funct. Bioinforma.* **75**, 430–441 (2009).
52. A. Wang, M. Levi, U. Mohanty, P. C. Whitford, Diffuse ions coordinate dynamics in a ribonucleoprotein assembly. *J. Am. Chem. Soc.* **144**, 9510–9522 (2022).
53. P. Eastman, R. Galvelis, R. P. Peláez, C. R. A. Abreu, S. E. Farr, E. Gallicchio, A. Gorenko, M. M. Henry, F. Hu, J. Huang, A. Krämer, J. Michel, J. A. Mitchell, V. S. Pande, J. P. Rodrigues, J. Rodriguez-Guerra, A. C. Simmonett, S. Singh, J. Swails, P. Turner, Y. Wang, I. Zhang,

J. D. Chodera, G. De Fabritiis, T. E. Markland, OpenMM 8: Molecular dynamics simulation with machine learning potentials. *J. Phys. Chem. B* **128**, 109–116 (2024).
54. A. B. De Oliveira, V. G. Contessoto, A. Hassan, S. Byju, A. Wang, Y. Wang, E. Dodero-Rojas, U. Mohanty, J. K. Noel, J. N. Onuchic, P. C. Whitford, SMOG 2 and OpenSMOG: Extending the limits of structure-based models. *Protein Sci.* **31**, 158–172 (2022).
55. J. Jackson, K. Nguyen, P. Whitford, Exploring the balance between folding and functional dynamics in proteins and RNA. *Int. J. Mol. Sci.* **16**, 6868–6889 (2015).
56. H. Yang, P. Bandarkar, R. Horne, V. B. P. Leite, J. Chahine, P. C. Whitford, Diffusion of tRNA inside the ribosome is position-dependent. *J. Chem. Phys.* **151**, 085102 (2019).
57. P. P. Cherepanov, W. Wackernagel, Gene disruption in *Escherichia coli*: TcR and KmR cassettes with the option of Flp-catalyzed excision of the antibiotic-resistance determinant. *Gene* **158**, 9–14 (1995).
58. M. Kitagawa, T. Ara, M. Arifuzzaman, T. Ioka-Nakamichi, E. Inamoto, H. Toyonaga, H. Mori, Complete set of ORF clones of *Escherichia coli* ASKA library (a complete set of *E. coli* K-12 ORF Archive). *DNA Res.* **12**, 291–299 (2006).

Acknowledgments: We thank D. Herschlag, R. Sauer, and D. Kahne for insightful comments. **Funding:** This work was supported by the following: National Institutes of Health grant R01GM12650 (to K.C.K.), National Institutes of Health grant R35GM153502 (to P.C.W.), National Science Foundation grant PHY2019745 (to P.C.W.), National Institutes of Health grant R35GM128836 (to K.S.K.), and National Institutes of Health grant R35GM156629 (to C.M.D.). We thank AMD for the donation of critical hardware and support resources from its HPC Fund that made this work possible. We also acknowledge support from the Northeastern University Explorer cluster and the Northeastern University Research Computing staff. **Author contributions:** Conceptualization: K.C.K., P.C.W., C.M.D., D.S., and M.C. Methodology: K.C.K., M.C., G.W., and C.M.D. Software: G.W. Validation: K.S.K., M.C., G.W., and C.M.D. Formal analysis: C.P., K.S.K., M.C., G.W., and C.M.D. Investigation: D.S., G.W., M.C., K.C.K., P.C.W., C.P., and E.U. Resources: P.C.W. and E.U. Funding acquisition: K.C.K., C.M.D., P.C.W., and K.S.K. Writing—original draft: D.S., M.C., K.C.K., G.W., and P.C.W. Writing—review and editing: D.S., K.C.K., G.W., P.C.W., C.M.D., C.P., and K.S.K. Visualization: K.C.K., C.P., K.S.K., M.C., G.W., P.C.W., and C.M.D. Supervision: K.C.K., M.C., P.C.W., and C.M.D. Project administration: K.C.K., K.S.K., M.C., and C.M.D. **Competing interests:** K.C.K. is a co-inventor on patent US 11,505,533 granted to Microbiotix Inc. and the Penn State Research Foundation on 22 November 2022, covering therapeutic use of MBX-4132. The other authors declare that they have no competing interests. **Data, code, and materials availability:** All data and code needed to evaluate and reproduce the conclusions in the paper are present in the paper and/or the Supplementary Materials. All new materials are described in Materials and Methods and can be obtained from the authors.

Submitted 23 January 2026
Accepted 2 July 2026
Published 7 August 2026
10.1126/sciadv.aef7696

ScienceAdvances

Ribosomal protein bL27 protects translating ribosomes from tmRNA-SmpB

Divyasorubini Seerpatham, George Wanes, Chathuri Pathirage, Mynthia Cabrera, Edu Usoro, Kristin S. Koutmou, Christine M. Dunham, Paul C. Whitford, and Kenneth C. Keiler

Sci. Adv. **12** (32), eaef7696. DOI: 10.1126/sciadv.aef7696